Materials Today: Proceedings 40 (2021) S28–S34

Contents lists available at ScienceDirect

Materials Today: Proceedings

journal homepage: www.elsevier.com/locate/matpr

Investigations on sputter deposited lithium nickel manganese oxide thin film cathodes for micro battery applications

Kosuri. Yellareswara Rao [a,*], Sabnavisu. Narasimham [a], Krishnaswamy. Narayan [b], Gowravaram. Mohan Rao [c]

[a] Dept. of Physics, Vignan's Institute of Information Technology, Visakhapatnam, Andhra Pradesh 530049, India
[b] Dept. of Electronics and Communication Engineering, Sai Vidya Institute of Technology, Bangalore, Karnataka 560064, India
[c] Dept of Instrumentation and Applied Physics, Indian Institute of Science, Bangalore 560012, India

ARTICLE INFO

Article history:
Received 13 February 2020
Received in revised form 9 March 2020
Accepted 11 March 2020
Available online 9 April 2020

Keywords:
Thin films
Sputtering
Li-ion battery cathodes
XPS
Electrochemistry

ABSTRACT

Lithium manganese oxide thin films have been deposited on nickel (Ni) and platinum (Pt) coated stainless steel substrates at room temperature using powder target by Radio Frequency (rf) reactive magnetron sputtering. The samples are exposed to heat treatment at 500 °C to form crystalline phase. Nickel and platinum thin film coatings have been carried out using direct current (DC) sputtering. X-ray diffraction (XRD), X-ray photoelectron spectroscopy (XPS), scanning electron microscopy (SEM) and electrochemical characterizations have been carried out. XPS spectra indicate the presence of all elements present in the powder target. A discharge capacity of 54 μAh μm^{-1} cm^{-2} and 48 μAh μm^{-1} cm^{-2} has been obtained from charge discharge studies in the potential range 2.0 to 4.4 V for the thin film samples deposited on Ni and Pt coated SS substrates correspondingly Charge discharge cycles are conducted up to 40 cycles.

1. Introduction

Li-ion rechargeable batteries represent one of the most prominent research areas for energy storage applications today. Owing to its long cycle life, high energy density etc., it has become indispensable in microelectronics and portable electronics power requirements [1–4]. The well-known cathode layers such as $LiCoO_2$, $LiMn_2O_4$, $LiFePO_4$ have remarkable discharge capacity, longer cycle life and operate in the potential range 3.0–4.2 V vs Li/Li^+. The next generation Li ion battery electrodes should be non-toxic, environment friendly and inexpensive for faster commercialization. The search for high voltage cathodes in bulk form as well as in the thin film form has attracted the electrochemical research community to fabricate high voltage cathodes. Recently, there are several reports on manganese based oxides with the composition Li_xMnO_y and $LiMn_xM_yO_z$ (M = Ni, Co, Cr) with spinel structure to provide high power density and high discharge capacity [5–8]. Among them, the promising material is $LiNi_xMn_yO_4$, which has high potential, long cycle life, high capacity [8–12]. In addition, the spinel structure of $LiNi_xMn_yO_4$ provides a three dimensional pathway for the diffusion of Li-ions, with high potential and discharge capacities of the order of 120 mAh g^{-1} in bulk powder form. Another Li-rich manganese based cathode Li_2MnO_3 was synthesized by several groups and studied its electrochemical activity [13–16]. Acid leaching process was performed to modify the structure with partial removal of Li_2O or Li_2O_2 to transform into $Li_{2-x}MnO_{3-y}$ [13–16]. The galvanostatis cycling studies provided the highest discharge capacity of 230 mAh g^{-1} [15–17]. Because of higher Mn content in the material, it is also cost effective as compared to cobalt based chemistry and due to lesser density of the manganese, the volumetric capacity also improves. It was reported that during the annealing treatment Ni diffuses through grain boundaries or lattice diffusion [18] and would give the $LiNi_xMn_yO_z$ composition. Diffusion properties of Ni were reported, and it was stated that Ni atoms diffuse either by grain boundary or lattice diffusion [18,19]. Since Ni^{2+} approximately has the same ionic radii as Li^+, it facilitates easy cation mixing and some of the Li^+ are occupied by Ni^{2+} in the structure [10]. When the substrate is heated to 500 °C, Ni can diffuse into lithium manganese oxide films and

* Corresponding author.
E-mail address: kyrao.2006@gmail.com (Kosuri. Yellareswara Rao).

https://doi.org/10.1016/j.matpr.2020.03.255
2214-7853/

can enhance the performance of the cathode layer. The merits of powder sputtering have also been reported earlier [20]. Less consumption of the material, slightly higher deposition rates and ease of making mixed oxides cathodes are the prominent advantages of powder sputtering. Electrochemical investigations of thin film samples carried out on the plain SS substrate (uncoated) resulted in lower potential and faster capacity decay and it was also reported that the addition of conductive additives to different cathode materials results in improved electrochemical performance due to decrease of contact resistance [22]. We choose Pt and Ni as interfacial metallic layer deposited [21,22] on SS substrates of equal thickness. In the recent literature $LiNi_xMn_yO_z$ ($x \sim 0.5$, $y \sim 1.5$) and substituted counterparts have been investigated extensively in large number because of high potential window (>4.5 V) and high capacity in bulk form (120–140 mAh g^{-1}) [23,24].

The main objective in the current work is to investigate the phase, surface analysis and electrochemical performance of lithium rich manganese oxide thin film samples deposited on Ni and Pt coated SS substrates. In case of Ni, due to its diffusive properties following annealing treatment, it could facilitate the formation of $LiNi_xMn_yO_z$ thin film phase compound. Similarly, Pt is a good choice in battery research due to higher electronic conductivity and chemical inertness. Hereafter the film deposited on Ni coated substrates is abbreviated as LMNO and the film deposited on Pt coated substrates is termed as LMO.

2. Experimental procedure

2.1. Thin film preparation using powder target of $Li_{2-x}MnO_{3-y}$

$Li_{2-x}MnO_{3-y}$ powder was prepared using acid treatment of as prepared Li_2MnO_3 powder followed by heat treatment as reported [17,25]. Approximately 20 g of the lithium rich manganese oxide powder was used to prepare the powder target and spread in a copper support plate having a trench of distance 4 mm. The as prepared target made from synthesized powder was used for preparation of thin films in a vacuum chamber having a base vacuum of 10^{-6} mbar. Steel substrates (SS304) having 2 mm thickness are used for film deposition having Ni and Pt as conductive layer. Ni and Pt films were deposited by DC sputtering and lithium manganese oxide film was deposited by rf sputtering (100 W, 13.5 MHz). The process values utilized for the film deposition are stated in Table 1. Substrate rotation was active during sputtering for uniform deposition. The thickness of LMO films is 100 nm–120 nm approximately. A schematic of implementing powder target for the thin film deposition is shown in Fig. 1 (inset shows copper backing plate, 75 mm dia, 4 mm groove). Pre-sputtering process was employed for prolonged time at lower rf powers (25 W) to enhance the compactness in the powder target and to avoid powder spill out during film deposition at required higher power.

2.2. Thin film characterization

X-Ray diffraction studies were conducted for thin film samples by Rigaku smart lab with copper kα radiation (40 mA, 30 KV). Film thickness was measured by stylus profilometer.Surface morphology studies were done using Zeiss ULTRA 55 SEM. X-ray Photoelectron spectroscopy (XPS) studies were carried out using Al electrode (1486.6 eV) SPECS PHOIBOIS 100 MCD analyser in an inert environment having vacuum 10^{-9} mbar. The reference peak for C 1 s is considered at 284.6 eV. Convolution and deconvolution of the high resolution spectra of constituent elements were carried out using CASA XPS software. Shirley type background is considered for peak fitting and quantification using Gaussian and Lorentzian functions.

To investigate the electrochemical performance cyclic voltammetry and chronopoeteniometry studies have been conducted using half cells. Half cells (homemade Swagelok cells) consist of LMO thin film as working electrodes immersed in the liquid electrolyte containing 1 M $LiPF_6$ in EC:DEC:DMC. The size of the electrode is 12 mm. The oxygen and moisture levels are sustained at <1 ppm. Galvanostatic charge discharge studies were conducted in the potential range 2.0–4.4 V. A current density of 25 μA cm^{-2} used while testing half cells. Specific discharge capacity is calculated after measuring thickness and area of the electrode used in half-cell preparation. All the electrochemical experiments were performed twice to check the repeatability of the results and conducted at room temperature (27 ± 1 °C).

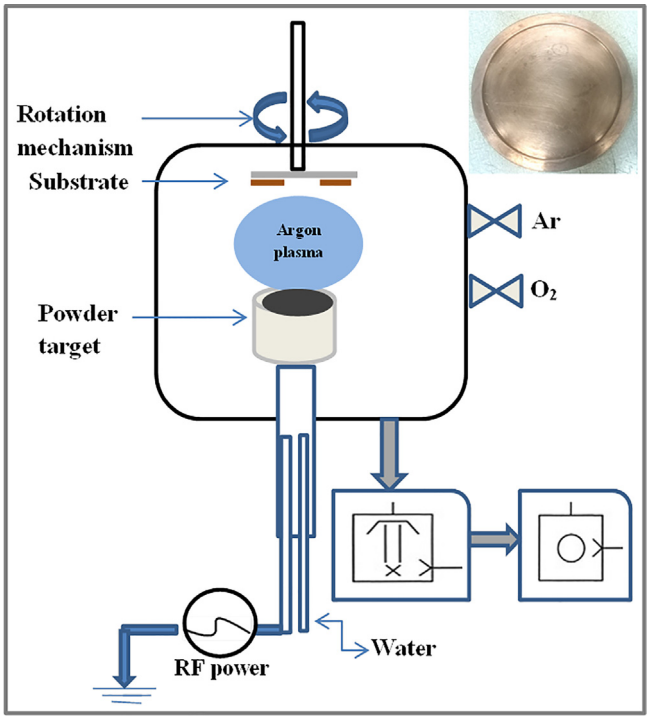

Fig. 1. Schematic of powder sputtering (inset shows copper backing plate, 75 mm dia, 4 mm trench).

Table 1
Experimental process parameters for LMO thin film preparation.

Deposition parameter	Value
Pressure	2.0×10^{-6} mbar
Working pressure	$2–4 \times 10^{-3}$ mbar
Working gas	60 SCCM (54 Ar 6 O_2)
Power density	2.2 W/cm^2
Substrate to target distance	5 cm

3. Results and discussion

3.1. Structural studies

XRD patterns of Li_2MnO_3, $L_{2-x}MnO_{3-y}$ powder, LMO film on Pt and Ni coated SS substrate are presented in Fig. 2(i–iv) respectively. The XRD pattern of Li_2MnO_3 agrees well with the JCPDS File No. 84-1634. The (0 2 0) and (1 1 0) reflections from the XRD pattern indicate layered structure. The XRD pattern of Li_2MnO_3 and acid treated powder ($Li_{2-x}MnO_{3-y}$) are looking different since there will be considerable loss of Li after acid treatment to transform into new compound $Li_{2-x}MnO_{3-y}$ as reported earlier [15,16,25]. As seen

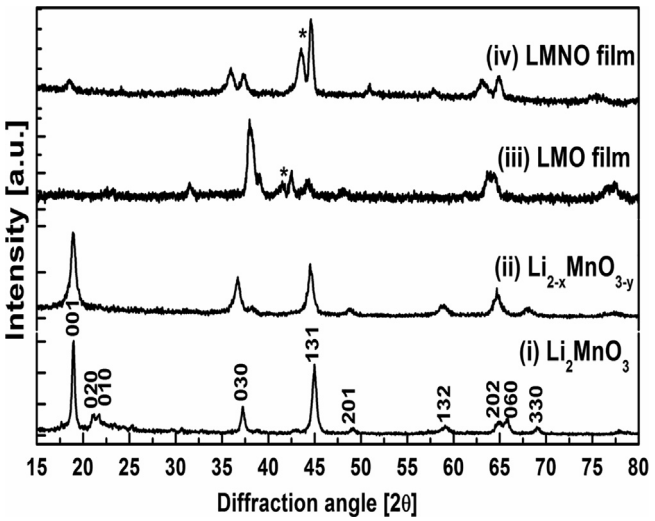

Fig. 2. XRD pattern of (i) Li_2MnO_3 (ii) $Li_{2-x}MnO_{3-y}$ powder target (iii) LMO film and (iv) LMNO film.

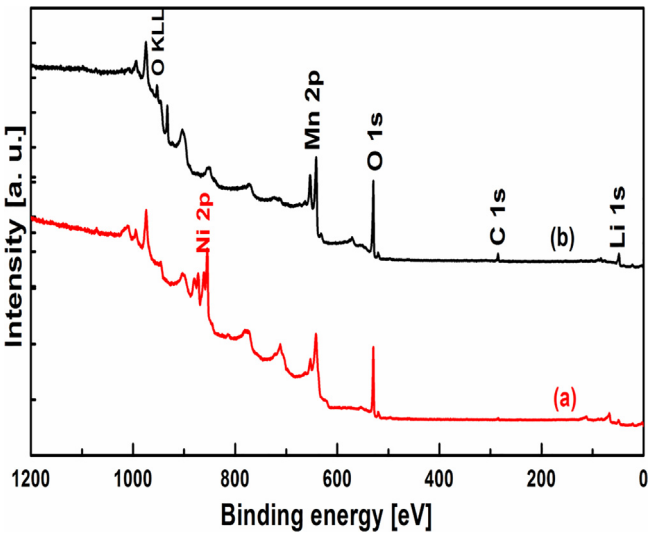

Fig. 4. XPS survey spectra of the film (a) LMNO (b) LMO film deposited at 100 W rf power and recorded at 30 eV pass energy.

from the patterns of Fig. 2 curve (ii) and (iv), the reflection at 37.3° and 64° corresponds to the NiO phase present in the film. We speculate that the Ni gets oxidised during the annealing process. In case of curve (iii) platinum reflections appeared at $2\theta \sim 38.8°$ and 44.5° and the reflection at 18.3°, which is present in all other samples, is absent. The reflection that corresponds to substrate is marked at 44.2°. The surface morphology of the film on Ni and Pt coated substrates are shown in Fig. 3(a) and (b) correspondingly. Clear tetrahedral type morphology is seen in both samples with well dispersed nearly uniform grains within the range 50–150 nm.

3.2. Surface analysis

The XPS survey spectra of films are shown in Fig. 4 taken with energy of 30 eV and with energy step of 0.5 eV using Al kα anode. From the comparison of two survey spectra, it is confirmed that Ni is diffused during annealing treatment in to LMO thin film because the analysis depth of XPS is well below 10–15 nm. More over the elements present in the bulk powder such as manganese, oxygen and lithium are also seen in the Fig. 4(a) and (b). In case of high resolution spectra of constituent elements, after deconvolution the resolved peaks are indicated as component 1, 2 for both thin film samples and taken at 10 eV energy.

Extended resolution XPS spectra of LMNO and LMO films are presented in the Figs. 5 and 6 correspondingly. In case of Fig. 5, Ni 2p, Mn 2p, O 1 s and Li 1 s have been measured at reduced pass energy step and presented in the Fig. 5(a), (b), (c) and (d) respectively. Scans are repeated to get good resolution in the specified energy range.

De-convolution of the spectra was carried out using CASA XPS software. As seen from the Ni 2p spectra, the spin orbit splitting for Ni 2p is 17.9 eV (Ni $2p_{1/2}$ at 854.2 eV and Ni $2p_{3/2}$ at 872.1 eV) in comparison to 17.6 eV corresponding to nickel oxidation state + 2 [7,9,26,27]. We observed satellite peaks at 863.5 eV and 883.2 eV. The spin orbit split for manganese and nickel, 11.6 eV and 17.9 eV respectively, are in agreement with the spin orbit split dependence on atomic number [28,29]. The origin of satellites peaks has also been reported to be because of the multiple splitting of energy levels in transition metal elements, which have unpaired electrons in outer shells through shake up or shake off mechanisms [29,30]. The O 1 s binding energy positions are located at 529.4 eV and 531.3 eV as seen from the Fig. 5(c). The oxygen from the crystalline structure is located at 529.4 eV (O

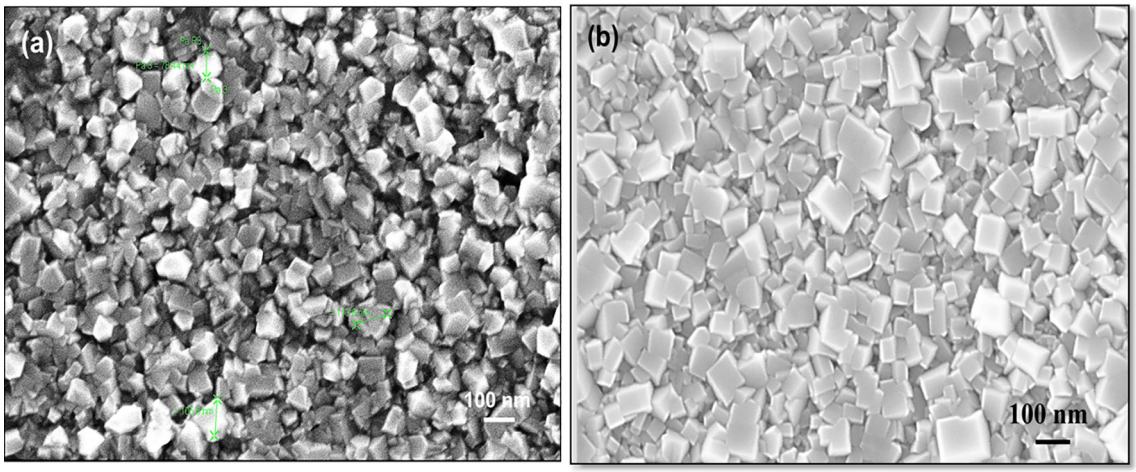

Fig. 3. Surface morphology of (a) LMNO (b) LMO thin film annealed at 500 °C for one hour.

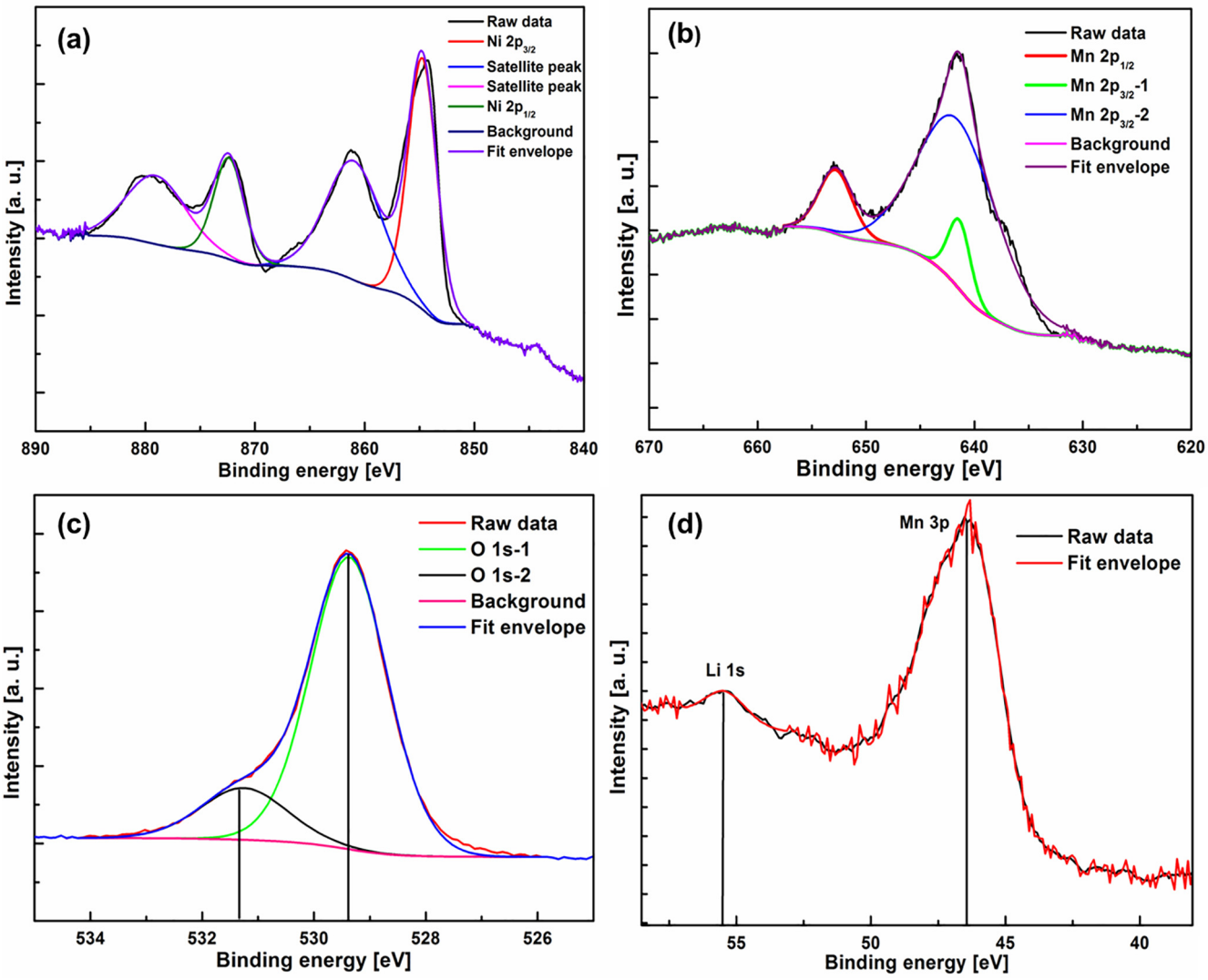

Fig. 5. (a) Ni 2p high resolution spectra (b) Mn 2p high resolution XPS spectra (c) O 1 s high resolution XPS spectra (d) Li 1 s high resolution XPS spectra of LMNO films recorded at a pass energy of 10 eV deposited at 100 W RF power.

1 s– component 1) and the surface adsorbed oxygen (OH=O, O–C) is located at 531.3 eV (O 1 s– component 2). The measured energy values coincide with the earlier reports [26–28].

Extended resolution spectra of Mn 2p, O 1 s and Li 1 s of LMO film are presented in Fig. 6(a), (b) and (c) correspondingly. Mn 2p doublet is observed due to spin orbit splitting. Mn $2p_{3/2}$ exhibits two peaks after de convolution which is indicated as components in Fig. 6(a) and Mn $2p_{1/2}$ is seen at 652 eV. O 1 s is also resolved into two components at 528.7 eV and 530.6 eV. Li 1 s is observed at 53 eV along with Mn 3p at 49 eV after deconvolution. It is clear that XPS binding energy values for Ni and Mn are in good agreement with that of the $LiMn_{1.5}Ni_{0.5}O_4$ derivative compounds from earlier reports [26–28]. Hence, it is speculated that diffusion of Ni facilitates the $LiNi_xMn_yO_z$ type phase formation in our case. The quantification of Lithium based compound is trivial, because most of the Li 1 s signal overlaps with Mn 3p and Ni 2 s following the physics of photoemission from Li (low cross-section).

3.3. Electrochemical measurements

For Galvanostatic charge discharge studies, half cells were charged and discharged with persistent current density of 25 μA cm^{-2} to obtain discharge capacity of the electrodes in the potential range 2.0 up to 4.4 V. The half cells were given a holding time of 15 min before it starts discharging from higher potential. We observed the plateaus in the potential range 2.9–3.1 V corresponding to manganese oxidation state Mn^{+3} to Mn^{+4} and between 3.9 and 4.2 V corresponding to Ni^{+2} to Ni^{+4} oxidation change. It was reported that Ni oxidises during the initial charging from Ni^{2+} to Ni^{4+} in the potential window 4.2–4.8 V [11,12]. Charge discharge profiles are shown up to 40 cycles are shown in Fig. 7(a) and (b) for LMNO and LMO films respectively. Cyclic voltammetry is used to study the redox behaviour of the electrodes during oxidation and reduction (Fig. 7(c) and (d)). During cyclic voltammetry the cells are subjected to voltage pulse of specific scan rate (200 μV s^{-1}) in the specific potential window and studied the response. CV plots have shown reversible nature of redox reaction in the deposited film. During oxidation, peaks at 2.7–3.0 V correspond to oxidation of Mn, while peak at 4.0–4.4 V corresponds to oxidation of Ni. The measured values in the present work are in good agreement with the earlier reports [5,30–33]. As shown in Fig. 7(a) and (b), the deposited thin film samples represent the reversible behaviour of the intercalation and de-intercalation of Li-ions taking place at the surface of electrodes.

Rate capability studies were carried out for the half cells starting from 25 μA cm^{-2} up to 200 μA cm^{-2} to check the stability of the

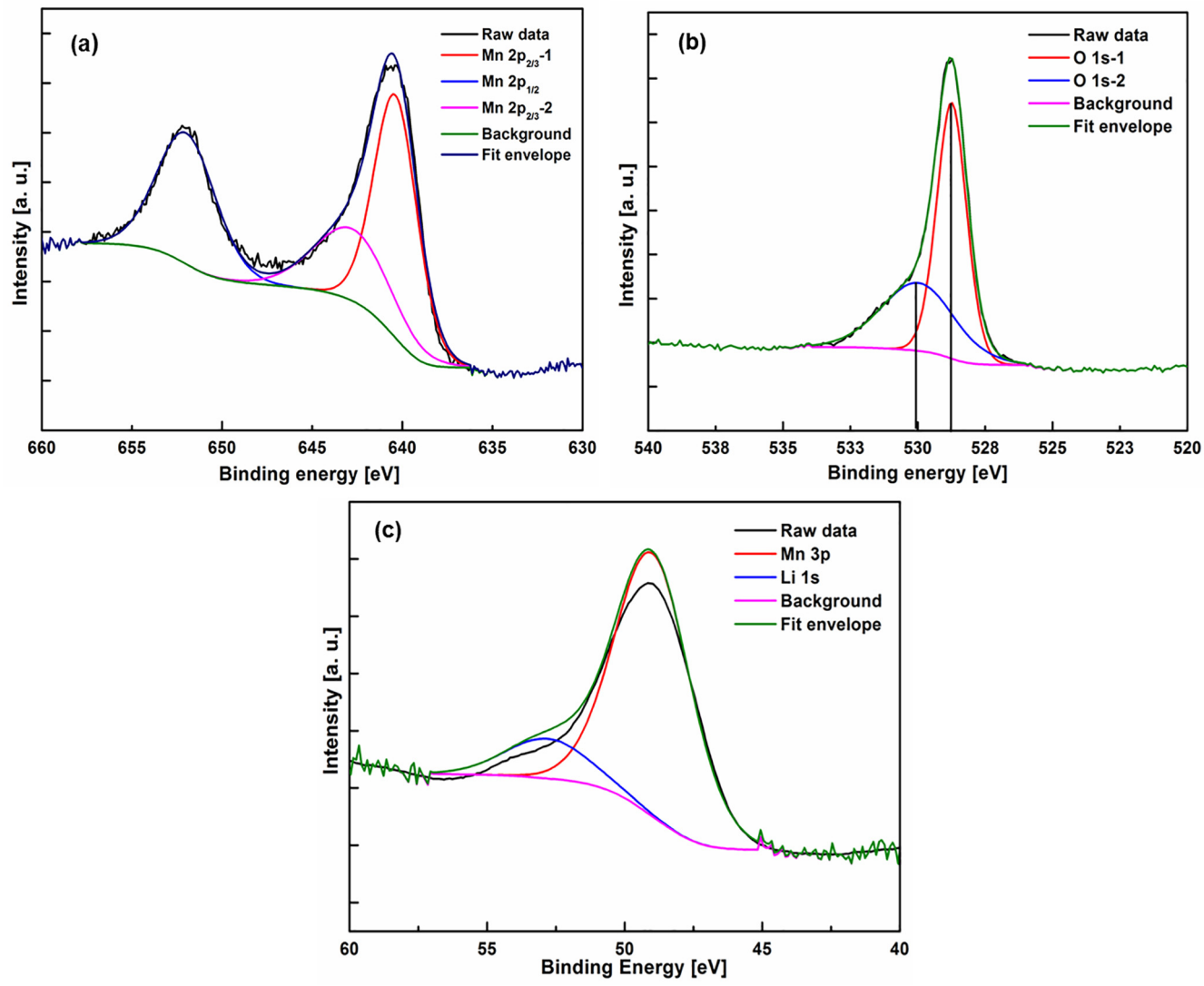

Fig. 6. (a) Mn 2p high resolution spectra (b) O 1 s high resolution spectra (c) Li 1 s high resolution spectra of LMO film recorded at a pass energy of 10 eV and deposited at 100 w RF power.

electrode during fast charge and discharge process. As seen from the Fig. 8(a) and (b), the discharge capacity decreases at high rate. In case of LMNO sample (Fig. 8(a)) 80% of the initial capacity has recovered during repetitive testing at the same current density where as in case of LMO film (Fig. 8(b)) it is 88% because of good electronic conductivity of Pt interfacial thin film layer. In case of LMNO film, it could be attributed to the changes in the $LiNi_xMn_y$-O_z phase composition, parasitic reaction at the cathode/electrolyte interface at high current. As expected the discharge capacity decreased with increase in the current because of increased cell resistance, morphological and structural changes originate during charging and discharging in both the samples. The cycle life tests of the LMNO and LMO films are shown up to 40 cycles in the Fig. 9 tested with current density value as 25 μA/ cm^2 during both charge and discharge.

Cycle life of the thin film electrodes is presented up to 40 cycles. LMNO film delivered high discharge capacity compared to LMO film as seen in the Fig. 9. At the end of 40 cycles discharge capacity reduction is less than 10% in both cases which indicates the stability of the deposited film during long cycle life.

The enhanced stability of the thin film cathodes during galvanostatic charge discharge tests is speculated due to processing method, improved contact between electrode/electrolyte and high surface area. Moreover thin film electrodes posses active material without any binders, facilitates reduced chances of unwanted reaction taking place at the electrode surface during testing. Hence the deposited thin film samples are good choice as cathode layers for fabrication of thin film battery.

4. Conclusions

Lithium manganese oxide thin films were deposited using radio frequency sputtering from powder target. XRD, XPS and electrochemical analysis were carried out for the prepared samples. XPS analysis indicates the presences of all elements in the powder are also present in the deposited film. Electrochemical half cells investigations using thin film electrode achieved 54 μAh μm^{-1} cm^{-2} and 48 μAh μm^{-1} cm^{-2} discharge capacities in the voltage range 2.0–4.4 V. Less capacity fading observed for the films deposited on Ni and Pt coated stainless steel substrates. Cyclic voltammetry results indicate the reversible nature of redox reactions. Hence the as prepared thin film samples finds potential application as cathodes layers in thin film Li-ion batteries.

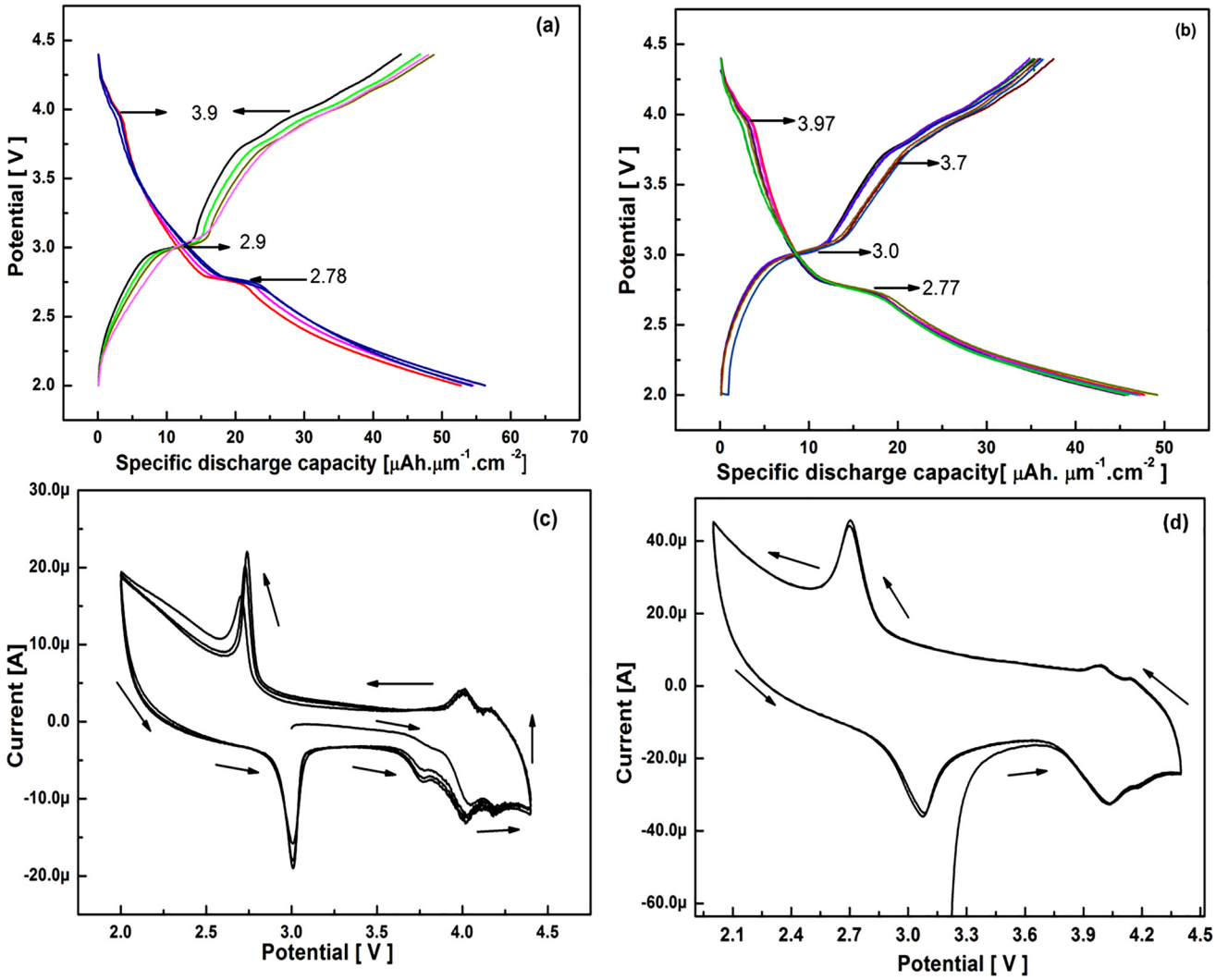

Fig. 7. Charge discharge profiles of (a) LMNO thin film electrodes (b) the LMO thin film electrodes using 25 μA cm^{-2} current density in the potential window 2.0–4.4 V vs Li/ Li^+ (after reaching the high potential 4.4 V cells are subjected to a holding time of 15 min). Cyclic voltammograms of (c) LMNO thin films (d) LMO thin films recorded at a scan rate of 200 μV s^{-1} in the potential window 2.0–4.4 V vs Li/ Li^+. (Arrow direction indicates scanning direction).

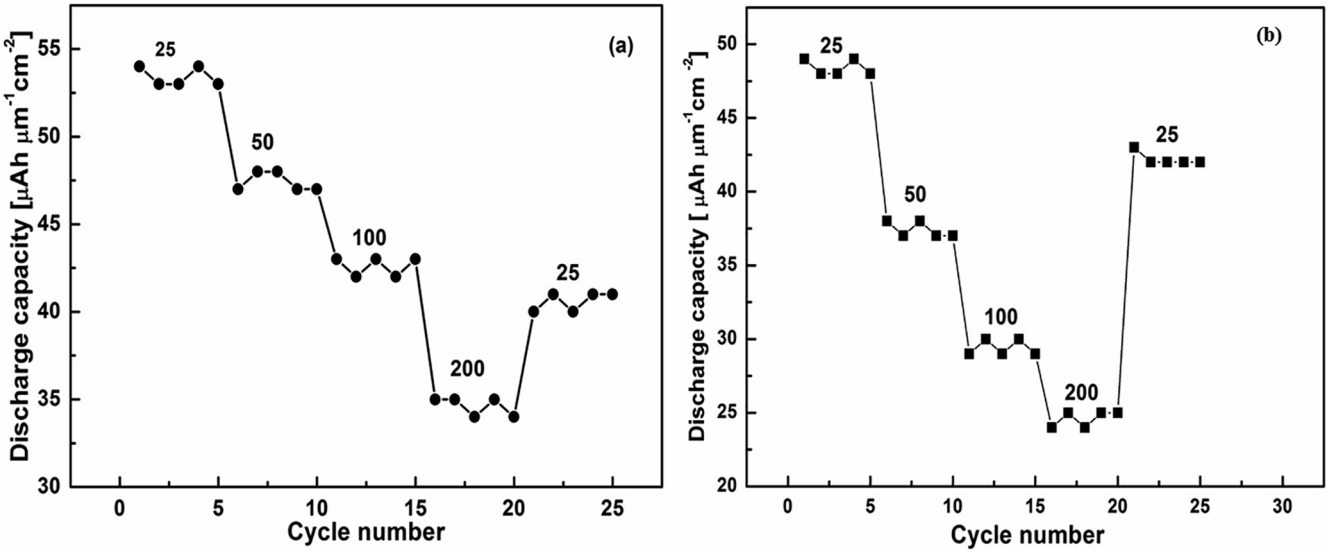

Fig. 8. . Rate capability studies of (a)LMNO thin film electrodes and (b) LMO thin film electrodes in the potential window 2.0–4.4 V vs Li/ Li^+ (indicated current density values are shown in μA cm^{-2}).

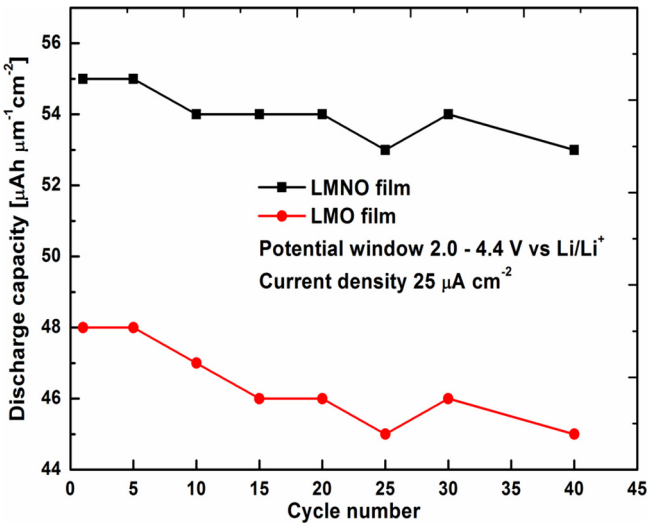

Fig. 9. Cycle life of the LMNO and LMO thin film samples.

CRediT authorship contribution statement

Kosuri. Yellareswara Rao: Conceptualization, Investigation. **Sabnavisu. Narasimham:** Writing - review & editing. **Krishnaswamy. Narayan:** Writing - review & editing. **Gowravaram. Mohan Rao:** Resources.

Declaration of Competing Interest

The authors declare that they have no known competing financial interests or personal relationships that could have appeared to influence the work reported in this paper.

Acknowledgements

KYR thank Department of Science and Technology, Science and Engineering Research Board (DST-SERB) for financial support (No. ECR/2017/001127). KYR also sincerely thank N. Munichandraiah, D. Shanmugasundaram and Penki Tirupathi Rao for their support.

References

[1] J.M. Tarascon, M. Armand, Nature 414 (2001) 359–367.
[2] M.S. Whittingham, Chem. Rev. 104 (2004) 4271–4302.
[3] Y.K. Sun, S.T. Myung, B.C. Park, J. Prakash, I. Belharouak, K. Amine, Nat. Mater. 8 (2009) 320–324.
[4] L.J. Fu, H. Liu, C. Li, Y.P. Wu, E. Rahm, R. Holze, H.Q. Wu, Solid. State. Sci. 8 (2006) 113–128.
[5] M. Gellert, K.I. Gries, J. Zakel, A. Ott, S. Spannenberger, C. Yada, F. Rosciano, K. Volz, B. Roling, Electrochim. Acta. 133 (2014) 146–152.
[6] S. Dou, J. Solid. State. Electrochem. 17 (2013) 911–926.
[7] H. Deng, I. Belharouak, R.E. Cook, H. Wu, Y.K. Sun, K. Amine, J. Electrochem. Soc. 157 (2010) A447–A452.
[8] D. Kim, S.H. Kang, M. Balasubramanian, C.S. Johnson, Electrochem. Commun. 12 (2010) 1618–1621.
[9] Y.K. Sun, S.T. Myung, M.H. Kin, J. Prakash, K. Amine, J. Am. Chem. Soc. 127 (2005) 13411.
[10] K.R. Ragavendran, L. Lu, B.J. Hwang, K. Barner, A. Veluchamy, J. Phys. Chem. C. 117 (2013) 3812–3817.
[11] K.R. Chemelewski, W. Li, A. Gutierrez, A. Manthiram, J. Mater. Chem. A. 1 (2013) 15334–15341.
[12] C.P. Grey, W.S. Yoon, J. Reed, G. Ceder, Electrochem. Solid. State. Lett. 7 (2004) A290–A293.
[13] J.B. Bates, N.J. Dudney, B. Neudecker, A. Ueda, C.D. Evans, Solid State Ionic. 135 (2000) 33–45.
[14] K.R. Chemelewski, D.W. Shin, W. Li, A. Manthiram, J. Mater. Chem. A. 1 (2013) 3347–3354.
[15] M.H. Rossouw, M.M. Thackeray, Mat. Res. Bull. 26 (1991) 463–473.
[16] A.D. Robertson, P.G. Bruce, Chem. Commun. 23 (2002) 2790–2791.
[17] T.R. Penki, D. Shanmugha Sundaram, N. Munichandraiah, J. Solid State Electrochem. 17 (2013) 3125–3136.
[18] A.R. Wazzan, J. App. Phys. 36 (1965) 3596–3599.
[19] J.C. Ciccariello, S. Poize, P. Gas, J. Appl. Phys. 67 (1990) 3315–3322.
[20] H. Kawasaki, D. Taniyama, S. Takeichi, T. Ohshima, Y. Yagyu, T. Ihara, Y. Tanaka, Y. Suda, J. Phys. Conf. Ser. 518 (2014) 012003.
[21] Y.H. Chen, C.W. Wang, G. Liu, X.Y. Song, V.S. Battaglia, A.M. Sastry, J. Electrochem. Soc. 154 (2007) A978–A986.
[22] M. Lengyel, G. Atlas, D. Elhassid, X. Zhang, I. Belharouak, R.L. Axelbaum, J. Electrochem. Soc. 161 (2014) A1023–A1031.
[23] H.D. Yoo, E. Markevich, G. Salitra, D. Sharon, D. Aurbach, Mater. Today 17 (2014) 110–121.
[24] M. Boutonnet, J. Kizling, P. Stenius, G. Marie, Colloids. Surf. 5 (1982) 209–225.
[25] D.Y.W. Yu, K. Yanagida, Structural analysis of Li_2MnO_3 and related Li- Mn- O materials, J. Electrochem. Soc. 158 (2011) A1015–A1022.
[26] L. Baggetto, D. Mohanty, R.A. Meisner, C.A. Bridges, C. Daniel, D.L. Wood, N.J. Dudney, G.M. Veith, RSC. Adv. 4 (2014) 23364–23371.
[27] H.Z. Zhang, Q.Q. Qiao, G.R. Li, S.H. Ye, X.P. Gao, J. Mater. Chem. 22 (2012) 13104–13109.
[28] G. Tan, F. Wu, J. Lu, R. Chen, L. Li, K. Amine, Nano Scale 6 (2014) 10611–10622.
[29] M.C. Biesinger, B.P. Payne, A.P. Grosvenor, L.M.W. Laua, A.R. Gerson, RStC Appl. Surf. Sci. 257 (2011) 2717–2730.
[30] D.D. Sharma, C.N.R. Rao, J. Electron. Spectrosc. Relat. Phenom. 20 (1980) 25–45.
[31] F. Wu, N. Li, Y. Su, L. Zhang, L. Bao, J. Wang, L. Chen, Y. Zheng, L. Dai, J. Peng, S. Chen, Nano. Lett. 14 (2014) 3550–3555.
[32] A. Boulineau, L. Simonin, J.F. Colin, C. Bourbon, S. Patoux, Nano. Lett. 13 (2013) 3857–3863.
[33] W. Zheng, X. Xu, L. Cheng, M. Shui, J. Shu, S. Gao, Z. Lu, L. Feng, Y. Ren, Ionics 19 (2013) 1509–1514.